PROCEEDINGS OF SPIE

SPIEDigitalLibrary.org/conference-proceedings-of-spie

Optimization and performance of multi-deformable mirror correction on the THD2 bench

Pierre Baudoz, Raphaël Galicher, Axel Potier, Olivier Dupuis, Simone Thijs, et al.

Pierre Baudoz, Raphaël Galicher, Axel Potier, Olivier Dupuis, Simone Thijs, Fabien Patru, "Optimization and performance of multi-deformable mirror correction on the THD2 bench," Proc. SPIE 10706, Advances in Optical and Mechanical Technologies for Telescopes and Instrumentation III, 107062O (10 July 2018); doi: 10.1117/12.2314089

SPIE.

Event: SPIE Astronomical Telescopes + Instrumentation, 2018, Austin, Texas, United States

Optimization and performance of multi-deformable mirrror correction on the THD2 bench

Pierre Baudoz*[a], Raphaël Galicher[a], Axel Potier[a], Olivier Dupuis[a], Simone Thijs[a], Fabien Patru[a]

[a]LESIA, Observatoire de Paris, Université PSL, CNRS, Sorbonne Université, Univ. Paris Diderot, Sorbonne Paris Cité, 5 place Jules Janssen, 92195 Meudon, France

ABSTRACT

High-contrast imaging (HCI) techniques appear like the best solutions to directly characterize the atmosphere of large orbit planets and planetary environments. In the last 20 years, different HCI solutions have been proposed based on coronagraphs. Some of them have been characterized in the laboratory or even on the sky. The optimized performance of these coronagraphs requires a perfect wavefront unreachable without active control of the complete electrical field (phase and amplitude) at the entrance of the instrument. While the correction of the phase aberrations is straight forward using deformable mirrors (DM), correcting amplitude defects is complex and still under study at the laboratory level. The next generation of HCI instrument either for ground-based (PCS instrument for ELT) or space-based (LUVOIR, HabEx) telescopes will require a practical and operational solution for amplitude corrections. The implementation of a DM located at a finite distance from the pupil is a simple solution that has been chosen by most of the projects. There have been only a few investigations on the optimization of the mirror positions for dedicated optical designs. In this paper, we give an intuitive approach that helps defining the best deformable mirror position in an instrument. Then, we describe its application to the THD2 and the performance in the laboratory that reaches a contrast level below 10^{-8} at distance larger than 6 λ/D.

Keywords: High Contrast Imaging, Deformable mirror, exoplanets, coronagraph

1. INTRODUCTION

High-contrast imaging (HCI) techniques are promising ways to allow a physico-chemical characterization of planets. It allows theoretically rejecting the light of the host star in order to observe directly planets that are up to 10 billion times fainter. But to achieve light rejection large enough to image rocky planets, minimizing the phase and amplitude defects upstream of the coronagraph is mandatory. This is possible with adaptive optics that compensate for atmospheric and instrumental aberrations. These active wavefront correction techniques are routinely used on large ground-based telescopes[1] and studies are pursued to apply them to space-based instruments[2]. A critical point of wavefront correction is the ability to make an unbiased measurement of wavefront errors upstream of the coronagraph. We have demonstrated in recent years that we were able to do this unbiased measurement with the technique called self-consistent camera or Self-Coherent Camera (SCC)[3,4,5]. This solution has been demonstrated on a test bench set up at LESIA-Observatoire de Paris (THD bench) by reaching contrast levels of the order of a few 10^{-8} both in monochromatic and for large spectral bandwith[6,7].

However, the level reached on the THD bench is limited by amplitude aberrations at the level of the order of 10^{-6} over the Full Dark Hole[8] (FDH), ie the full field of view where the Deformable Mirror (DM) should be able to correct phase effects. Since a DM creates only phase, we cannot correct for both phase and amplitude aberrations at the same time. To reach 10^{-8} level, we apply phase on the DM to correct the effects of the phase and the amplitude only in a half Dark Hole, ie half of the correcting area of the DM[7]. A few studies[9,10] have been pursued so far on the simultaneous correction of phase and amplitude but with relatively limited contrast levels[11]. In this paper, we study the implementation of a DM located at a finite distance from the pupil to optimize the correction on the THD bench. In this context, we first give a general approach to define the best mirror position in an instrument. Using this simplified analysis, we present the optimized solutions found for the upgraded THD2 design using 2 or 3 mirrors. After describing the method used to correct amplitude aberrations over the full field of view, we present performance in FDH.

Advances in Optical and Mechanical Technologies for Telescopes and Instrumentation III, edited by Ramón Navarro, Roland Geyl, Proc. of SPIE Vol. 10706, 107062O · © 2018 SPIE
CCC code: 0277-786X/18/$18 · doi: 10.1117/12.2314089

2. FORMALISM FOR ELECTRIC FIELD AT FINITE DISTANCE Z

2.1 Electric field at finite distance z and Talbot length

First, we want to estimate the effect of a DM as a function of the distance to this DM to better understand how to take advantage of Fresnel propagation to correct for phase and amplitude aberrations.

The complex amplitude describing the electric field at the origin z = 0 of the propagation distances is:

$$E_{z=0}(x) = E_0(x) = (1 + A(x))e^{i\phi(x)} \tag{1}$$

with $A(x)$ describing the amplitude aberrations (A is of zero mean) and $\phi(x)$ the phase aberrations. The variable x is a 2-D variable.

Assuming the aberrations of phase and amplitude are small enough to consider that we can develop at first order the effects of these aberrations.

$$E_0(x) = 1 + A(x) + i\phi(x) \tag{2}$$

This hypothesis is rather true for the THD bench. Without DM correction, phase aberrations were estimated around 10-15 nm before correction. After correcting these phase aberrations using 1 DM, the level of amplitude aberrations is of the order of 6% RMS on the amplitude (11% on the intensity).

The correction of the aberrations will be based on 2-D sine and cosine applied to the different DMs[12]. In this Fourier basis, each sine or cosine of period p applied in the pupil plane corresponds to two speckles offset by $p\lambda/D$ and $-p\lambda/D$ of the optical axis in the focal plane. The total phase can be described as a linear sum of these sines and cosines:

$$\phi(x) = \sum_p \left[\alpha_p \sin\frac{2\pi x}{p} + \alpha'_p \cos\frac{2\pi x}{p}\right] = \sum_p \left[\phi_p + \phi'_p\right] \tag{3}$$

To understand how a phase aberration converts into amplitude aberration, we only need to study a purely sinusoidal phase aberration introduced in z = 0: $\phi_p(x) = \alpha_p \sin\frac{2\pi x}{p}$ with α_p small enough to remain on the small defects assumption described above.

At z = 0, the electric field is a pure phase aberration:

$$E_0^p(x) = 1 + i\,\alpha_p \sin\frac{2\pi x}{p} = 1 + i\phi_p(x) \tag{4}$$

Assuming small aberrations, Zhou & Burge 2010[13] calculate the electric field at the distance z:

$$E_z^p(x) = 1 + \alpha_p \sin\frac{2\pi x}{p}.\left[\sin\frac{2\pi z}{z_T} + i\cos\frac{2\pi z}{z_T}\right] \tag{5}$$

with z_T, Talbot length defined by:

$$z_T = \frac{2p^2}{\lambda} \tag{6}$$

with λ the wavelength. In the case of a periodic grating, Talbot discovered that an image of a grating was repeated at regular distances as one moved away from it. This regular distance is called the Talbot length.
For all distances z such that $z = \frac{n\,z_T}{2}$, we find the same pure phase variation than at z=0:

$$E^p_{nz_T/2}(x) = 1 + i\,\alpha_p \sin\frac{2\pi x}{p} = E^p_0(x) \tag{7}$$

On the other hand, the phase vanishes and $E^p_0(x)$ is changed into a pure amplitude for the distances z such that $z = \frac{(2n+1)\,z_T}{4}$:

$$E^p_{(2n+1)z_T/4}(x) = 1 + \alpha_p \sin\frac{2\pi x}{p} \tag{8}$$

We therefore have a conversion of the phase in amplitude, which depends on the propagation distance z and on the period p of the aberration.

2.2 Talbot length in converging beam

We can also use the above equations in a convergent beam. Let's assume a telecentric system with large F/D (F/D>30) as described in Figure 1. The equivalent propagation distance for a converging beam can be calculated by applying Newton lens formula :

$$z_{eq} = \frac{F^2}{L} = \frac{F\,D}{d} \tag{9}$$

With L the distance between the plane of the aberrations and the focal plane and F the focal length of the lens placed downstream of the focal plane to re-image the pupil. The diameters D and d correspond to the diameter of the geometrical beam at the distance F and L respectively (D is the diameter of the pupil and d is the diameter of the DM required at the distance L from the focal plane). We can also define the equivalent period:

$$p_{eq} = \frac{F}{L}p = \frac{D}{d}p \tag{10}$$

The amplitude of the aberration remains obviously unchanged for L >> λ.
Note that the position upstream or downstream of the focal plane will not change the absolute value of the propagation distance but only the position of the equivalent plane upstream or downstream of the pupil. We see in Equation 5 that the sign of z will simply change the electric field to its conjugate.

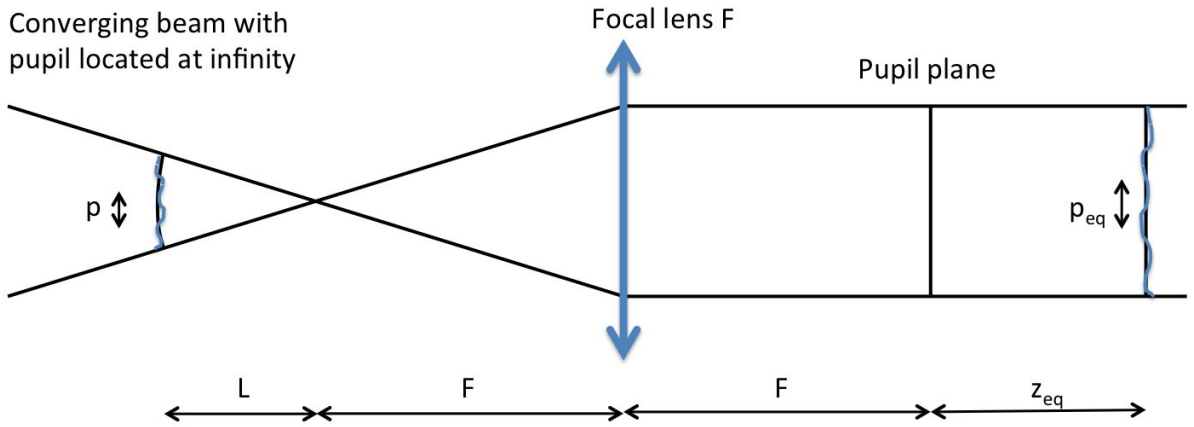

Figure 1: Geometry used to compare convergent beam aberrations and collimated beam aberrations. The lens is perfectly thin and can be replaced by a concave mirror.

2.3 Application to Amplitude correction

By placing a deformable mirror (DM_z) at a distance z from the pupil, it is therefore possible to create phase and amplitude in the pupil plane using DM_z as described in Equation 5. Choosing the right distance z for a given period of sine aberration, it is even possible to convert the pure phase introduced by a DM_z to pure amplitude as shown in Equation 8. However, for a given distance z and another period p, part of the p-periodic phase induced by DM_z will be converted into amplitude but the rest will remain phase and this phase will be multiplied by $\cos\frac{2\pi z}{z_T} = \cos\frac{\pi\lambda z}{p^2}$. Thus, the remaining phase shows a chromatic variation that cannot be fully corrected by another deformable mirror DM_{pup} that is located in the pupil plane. This effect can be used to correct for chromatic variation of the phase. Since the conversion from phase to amplitude is faster than the chromatic phase change (sinus versus cosinus for $z \ll z_T$), this chromatic effect should be low if amplitude aberrations to be corrected are not too strong. In this paper, we will focus our study on amplitude correction in short spectral bandwidth.

It is impossible to find a distance z that satisfies this need for a continuous range of period since z_T depends on the period p. In a real case, introducing sinusoids on a DM_z far from the pupil plane will therefore introduce both phase and amplitude. We will assume that the phase introduced can always be compensated by another DM_{pup} that is located in the pupil plane. We are therefore interested only in the amplitude effects that can be introduced by positioning a DM_z at a distance z from the pupil. This DM_z will introduce pure phase sine functions as defined in Equation 4. From Equation 5, we can define the amplitude correction that such a DM_z can create at the level of the pupil:

$$A_p^{DM_z}(x) = \alpha_p \sin\frac{2\pi x}{p}.\sin\frac{2\pi z}{z_T} = \phi_p^{DM_z}(x).\sin\frac{2\pi z}{z_T} \tag{11}$$

The phase-amplitude conversion is weighted by an efficiency term (in sine) which vanishes for z = 0 and $z = \frac{n\, z_T}{2}$ with n an integer.
In Figure 3, we plot the conversion efficiency as a function of the period of the aberrations and for different distances z. We also overlay in red the range of periods that can be corrected by a 30x30 DM. This range is defined for a DM with N actuators by:

$$d_{act}\sqrt{2} < p_N < N.d_{act} \tag{12}$$

With d_{act} the pitch separating 2 actuators. For a 30x30 DM and a pupil of 9 mm (THD bench values), N = 30, d_{act} = 0.3 mm, thus, 0.42 mm < p_{30} < 9.0 mm.

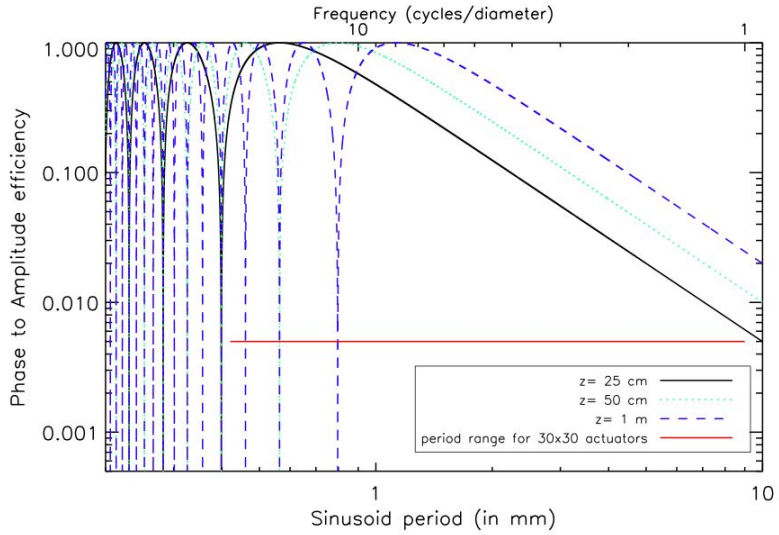

Figure 2: Efficiency of phase-amplitude conversion as a function of the sinusoid period for 3 propagation distances (25 cm, 50 cm, 1 m). λ = 635 nm.

The Figure 2 shows that the conversion efficiency reaches zero for several frequencies reachable by a 30x30 DM if the propagation distance is greater than 25 cm. Thus, 25 cm is the largest propagation distance if we want to correct completely the amplitude in the FDH. We also see that the efficiency is very low (few %) for the largest periods (low spatial frequencies) even for z= 1m. Therefore, for small z, correction of low frequencies amplitude defects requires large phase on the DM_z. Since our study is based on the assumption of linearity of the introduced defects, the phase introduced by the DM_z should stay well below 1 radian. As noted earlier, large phase outside of the pupil will also introduce strong chromatic phase variation. Besides, it is simpler for the correction to remains in the linear zone (recording of interaction matrix, closed-loop behavior).

3. AMPLITUDE CORRECTION ON THE THD2 BENCH

3.1 Estimation of the amplitude level to be corrected on THD2

To estimate the level of phase required to correct a given amplitude aberration, we first estimate the amplitude aberrations to be corrected. Using the intensity measured on the THD2 bench, we estimate the amplitude of the sine and cosine necessary for the correction. The aberrations of measured amplitudes are of the order of 6% RMS (on the amplitude, 11% RMS on the intensity) and explain very well the limitation in contrast for the THD bench (that used only one DM_{pup} in pupil plane and could does not correct for these aberrations in FDH[12]).

Let $A_p(x) = A_p^0 \sin\left(\frac{2\pi x}{p}\right)$ represents an amplitude aberration of period p measured on the bench. We assume a pure phase sine here but we can handle cosine the same way. A_p^0 is estimated using the Fourier transform of the modulus of the electric field which is measured on the bench (the modulus is estimated from the recorded intensity). The mean and maximum A_p^0 are shown in Figure 3.

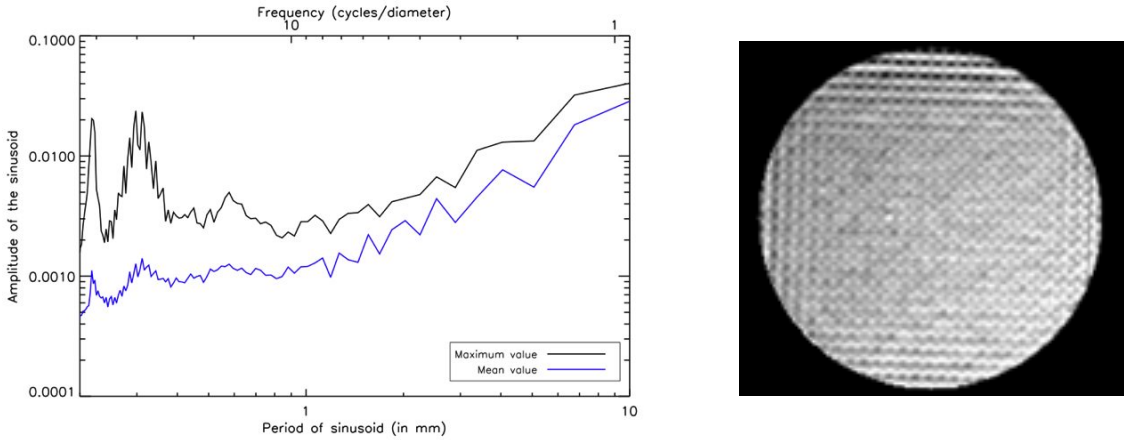

Figure 3: Right: Intensity measurement of the amplitude errors in the pupil plane of the THD bench. Left: Level of the measured amplitude aberration projected on the Fourier basis (sines and cosines). In blue, azimuthal average value. In black, maximum value. Pupil image recorded at λ = 635 nm.

We will have a perfect correction if:

$$A_p(x) = A_p^{DM_z}(x) \leftrightarrow A_p^0 = \alpha_p . \sin\frac{2\pi z}{z_T} = \frac{2\pi\delta^p}{\lambda} . \sin\frac{2\pi z}{z_T} \tag{13}$$

With δ^p, the maximum stroke amplitude of the actuators of the DM_z for a period p.

We see that the distortion of the mirror depends on the distance of Talbot and A_p^0.

$$\delta^p = \frac{A_p^0 \lambda}{2\pi \sin\frac{2\pi z}{z_T}} \tag{14}$$

By replacing A_p^0 in equation 14 by the measurements presented in Figure 3, we can deduce the stroke required on the DM_z for different propagation distances z (Figure 4). Note that for a small propagation distance (25cm), very strong strokes (>

1000 nm, > 10 radians) are required to correct the low spatial frequencies (large periods). In this case, we have deformations greater than the radian, which is no longer compatible with the assumption of the linearity of the defects. To correct the low frequencies, it is preferable to place the mirror at a much greater propagation distance but for these long distances, the high frequencies are no longer correctable because of the local minima of the phase-amplitude conversion efficiency function.

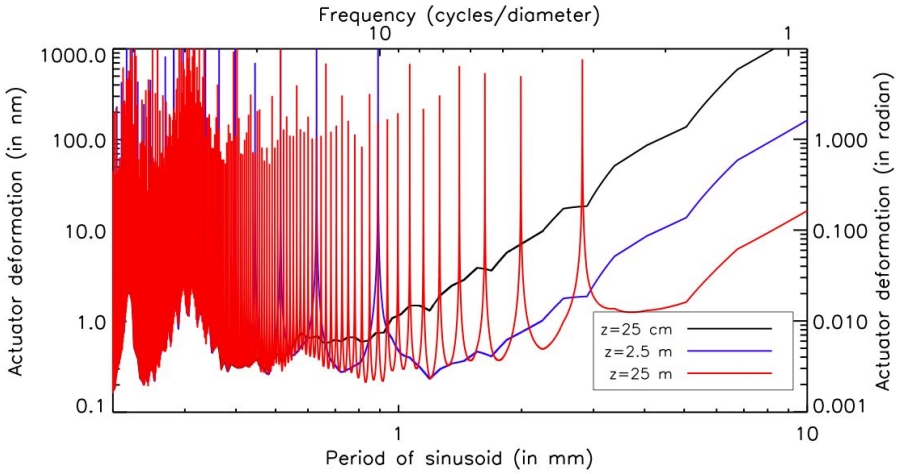

Figure 4: Value of the maximum deformation of the DM_z as a function of the period of the sinusoid (or spatial frequency) for three different propagation distances (0.25 m, 2.5 m, 25 m). $\lambda = 635$ nm.

3.2 Multi-DM configuration of the THD2 bench

We propose a solution to limit the non-linearity by splitting the correction of the amplitude aberrations on two deformable mirrors, DM1 correcting the high spatial frequencies (small periods) and DM2 correcting the low frequencies (large periods). The phase introduced by these mirrors and the phase due to the optics of the bench are corrected with a third mirror in a pupil plane (DM3). The solution proposed for THD2 can be described as below:

- 1 DM for high spatial frequencies (requiring many actuators) and placed at about 30 cm from the pupil (DM1)
- 1 DM for low spatial frequencies (requiring few actuators) and placed more than 2m away from the pupil (DM2)
- 1 DM to correct the phase aberrations only (with many actuators) and placed in the pupil plane (DM3)

To limit the size of the instrument, we choose to place DM2 in a converging beam. It has 2 advantages:

1) The effective pupil distance reaches 2.5m without increasing the size of the instrument.
2) In term of price, since we do not need a large number of actuators for this DM, we can use a smaller (less expensive) DM in the converging beam.

The optical design of the THD2 bench is then simply an upgrade of the THD bench where we add a reflection on DM1 located at 26.9 cm after the pupil plane and folding again the beam with DM2 located at 29.8 cm from the first focal plane of the bench (Figure 5). The bench has been upgraded with a Boston Micromachines 34x34 actuators at the location of DM1. DM2 will be a 12x12 actuators Boston Micromachines mirror but a flat mirror initially replaces it. The THD2 bench optical design is described in details in Baudoz et al. 2017[14]. The main components used for the tests described below are quickly recalled:

1. An optical fiber source that is fed by a laser diode fiber (@ 637 nm, 705 nm or 783.25 nm) or a white light source coupled with bandwidth filter. The tests performed in the paper used the 783.25 nm laser.
2. A fully reflective optical design creating 3 pupil planes where we place:

- (a) An unobscurated entrance pupil plane of 8.23 mm and a tip-tilt mirror
- (b) A Boston Micromachines deformable mirror of 32x32 actuators with a pitch of 0.3 mm.
- (c) Lyot stops of 8.1mm (98% filtering) or 6.5 mm (79% filtering) and several reference holes to allow SCC measurements

3. And 3 focal planes, two of which include:
   - (a) For the tests described in the paper, a monochromatic Four Quadrant phase mask(FQPM[15]) optimized for a wavelength of 783.25 nm
   - (b) A sCMOS camera of 2560x2160 pixels (400x400 used) with a readout noise of 2 e- and a Full Well capacity of 15 000 e-
4. A Boston Micromachines deformable mirror of 34x34 actuators with a pitch of 0.3 mm located at 26.9 cm away from the pupil
5. Simultaneous recording of the photometric flux injected on the bench to calibrate the photometry of the coronagraphic images.
6. A Lyot-based low-order wavefront sensor[16] used to stabilize the beam when recording the interaction matrix and during closed-loop correction.
7. A software (labview) that control all the elements of the bench (computer interaction, DM, motors, control loop, spectrometer, fluxmeter,…)

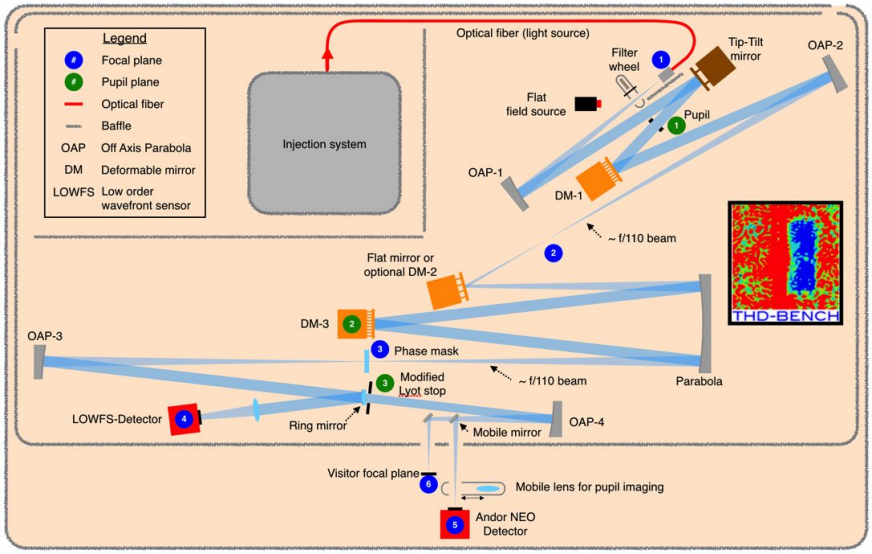

Figure 5: Physical implementation of the elements on the THD2 bench

3.3 Practical correction method with two DM

To test the correction capabilities of the multi-DM configuration, we need to estimate precisely the phase and amplitude aberrations upstream of the coronagraph. We have already proven that the focal plane wavefront sensor called Self-Coherent Camera (SCC) is very efficient to estimate very precisely the complete electric field[6,8]. The SCC uses part of the light diffracted by a focal mask outside of the Lyot stop to create fringes that encode the electric field in the focal plane. This encoding allows retrieving the effects of phase and amplitude of the beam upstream of the coronagraph[6]. To link the measured complex amplitude in the focal plane with the applied voltages on the DM, we build interaction matrix as described in Baudoz et al. 2012[14]. We chose to build an interaction matrix based on sine and cosine for each DM (here

DM1 and DM3). A control matrix can be calculated inversing both interaction matrix with a least square minimization using Singular Value Decomposition (SVD).

While correction of high frequency amplitude aberration is working with DM1 and DM3, we could not correct the low frequency aberrations with such an interaction matrix. Without DM2, it requires strong strokes from the DM1 mirror to correct low frequency amplitude aberrations. As only a small part of the phase introduced by DM1 is converted into amplitude for low spatial frequency, we need to use strong strokes when recording the interaction matrix. Doing so, DM1 also introduces a strong phase aberration in the pupil plane and thus, bright speckles in the focal plane. Measurement noise from these speckles prevents the measurement of the small amplitude effect in the focal plane. Thus, measuring the low frequency amplitude effect of DM1 requires the correction of the phase aberrations in the pupil plane so that the intensity of the bright speckles is minimized.

It is possible to perform this measurement if we record an interaction matrix of the amplitude effects of DM1 while DM3 is correcting the phase aberrations introduced by DM1. We applied this solution to record a non-linear interaction matrix for DM1 and then correct in the full field even the lowest amplitude frequencies. The correction steps are described below:

1. Recording Interaction matrix with DM3 (as described in Baudoz et al. 2012[14] using 960 Fourier modes)
2. Full Dark Hole correction with DM3
3. Nonlinear interaction matrix of DM1 for low order aberrations (30 Zernike modes) with DM3 correcting phase in closed loop. The amplitude of the DM1 voltages is applied as a ramp during a 20 to 50 iterations of the DM3 loop, then we record the electric field for each mode (Figure 6, Left)
4. Correction of low amplitude aberrations with DM1 to correct the low amplitude aberrations while DM3 correct the phase introduced by DM1 (Figure 6, Right)
5. Linear interaction matrix of DM1 (using 960 Fourier modes)
6. Correction of high frequencies with both DM1 and DM3 (Figure 6, Right also but with a different control matrix for DM1)

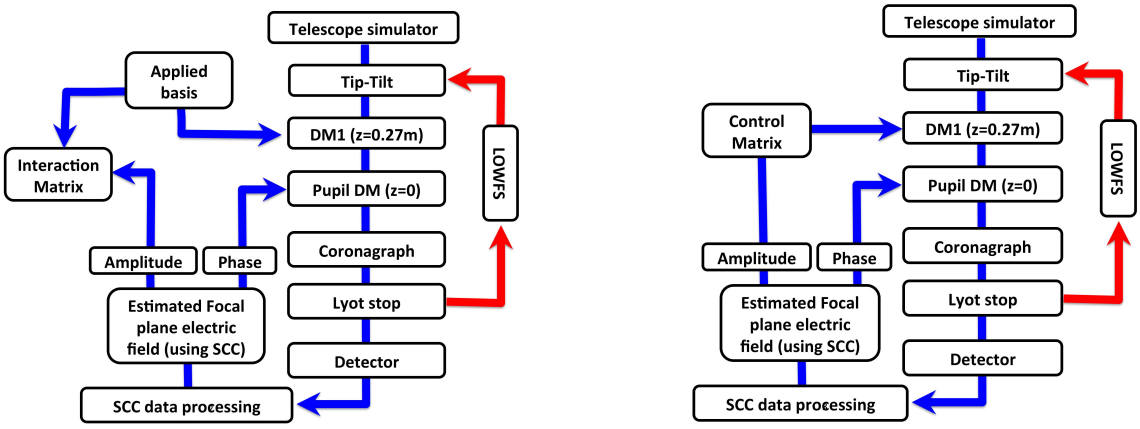

Figure 6: Left: Recording of a non-linear interaction matrix by applying strong phase defects on DM1 to measure the amplitude effect. The LOWFS[16] loop is also closed during interaction matrix recording to keep the beam well stabilized. Right: Closed-loop correction separating the estimated phase and amplitude to control one DM per effect. LOWFS loop is open to be able to optimize the centering of the beam on the coronagraph.

3.4 Performance with two DM on the THD2

We applied the process of correction described above for two bench configurations, both using a FQPM coronagraph with a laser at 783.25 nm with either a filtering of the Lyot stop of 98% or 79% in diameter. A linear polarizer is located at the entrance of the camera to suppress limitation from instrumental polarization. The performance reached is estimated

by measuring the azimuthal standard deviation of the coronagraphic images that were normalized with the maximum value of the PSF image when shifted away from the coronagraph center. The correction is better for 78% filtering with the Lyot stop (Figure 7). We reach a level below 10^{-8} over the FDH at a distance larger than 6 λ/D. This is an improvement by a factor 20 to 100 compared to the typical Full Dark Hole limitations with one DM that is drawn also in Figure 7. Compared to Half Dark Hole performance[8], we are reaching the same contrast at the same distance of the coronagraph axis but with the access to the full field of view.

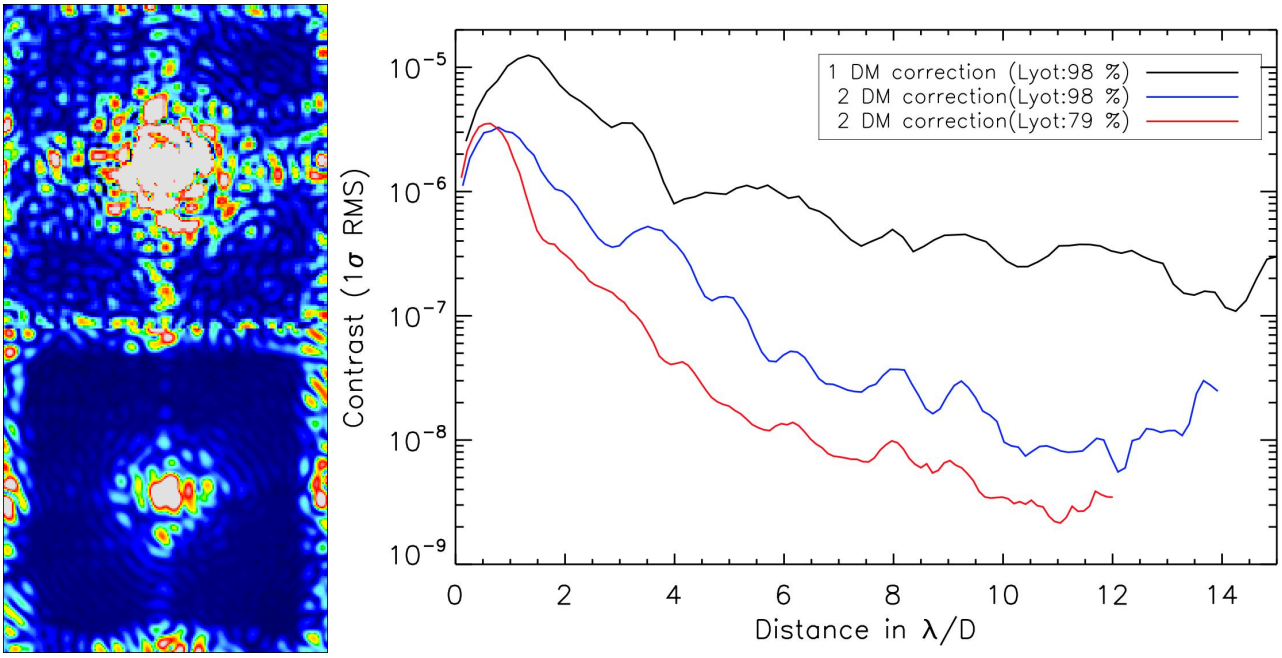

Figure 7: Left-top: 1 DM correction (Lyot=98%). Left-bottom: 2 DM correction (Lyot=98%). Right: Azimutal standard deviation on the coronagraph image normalized with the maximum value of the PSF image when shifted away from the coronagraph center. Black line corresponds to the top-left image. Blue line corresponds to the bottom-left image. Red line corresponds to a configuration where the Lyot stop has been reduced to 79% of filtering.

4. CONCLUSION

We defined the basis of a simple and intuitive approach for the correction of amplitude aberrations using multi deformable mirrors. We applied this analysis to upgrade our test bench and conclude that an interesting solution was to use using two deformable mirrors to correct of amplitude effects, one being dedicated to low spatial frequencies and the other to the median and high spatial frequencies and a third DM located in the pupil for the correction of the phase. The upgraded bench with two DM initially showed that the performance is improved by two orders of magnitude in Full Dark Hole correction with contrast better than 10^{-8} reached at distance larger than 6 λ/D.

ACKNOWLEDGMENTS

The authors would like to thank the LABEX ESEP and the IRIS OCAV from PSL University for providing funding for the THD bench development and the funding. ESEP (http://www.esep.pro) is focused on Space Exploration of Planetary Environments and IRIS OCAV (http://www.univ-psl-ocav.fr) is an interdisciplinary group working on the origin and conditions favorable to the emergence of life.

REFERENCES

[1] Sauvage, J.-F., Fusco, T., Petit, C., Costille, A., Mouillet, D., Beuzit, J.-L. et al., "SAXO: the extreme adaptive optics system of SPHERE (I) system overview and global laboratory performance", Journal of Astronomical Telescopes, Instruments, and Systems, Volume 2, id. 025003 (2016).

[2] Trauger, J., Moody, D., Krist, J., Gordon, B., "Hybrid Lyot coronagraph for WFIRST-AFTA: coronagraph design and performance metrics", Journal of Astronomical Telescopes, Instruments, and Systems, Volume 2, id. 011013 (2016).

[3] Baudoz, P., Boccaletti, A., Baudrand, J., and Rouan, D., "The self-coherent camera: a new tool for planet detection," in [IAU Colloq. 200: Direct Imaging of Exoplanets: Science Techniques], Aime, C. and Vakili, F., eds., 553–558 (2006).

[4] Galicher, R., Baudoz, P., and Rousset, G., "Wavefront error correction and earth-like planet detection by a self-coherent camera in space," Astronomy and Astrophysics 488, L9–L12 (2008).

[5] Galicher, R., Baudoz, P., Rousset, G., Totems, J., and Mas, M., "Self-coherent camera as a focal plane wavefront sensor: simulations," Astronomy and Astrophysics 509, A260000+ (2010).

[6] Mazoyer, J., Baudoz, P., Galicher, R., and Rousset, G., "High-contrast imaging in polychromatic light with the self-coherent camera," A&A 564, L1 (2014).

[7] Delorme, J. R., N'Diaye, M., Galicher, R., Dohlen, K., Baudoz, P., Caillat, A., Rousset, G., Soummer, R., and Dupuis, O., "Laboratory validation of the dual-zone phase mask coronagraph in broadband light at the high-contrast imaging THD testbed," Astronomy and Astrophysics 592, A119 (2016).

[8] Mazoyer, J., Baudoz, P., Galicher, R., Mas, M., and Rousset, G., "Estimation and correction of wavefront aberrations using the self-coherent camera: laboratory results," Astronomy and Astrophysics 557, A9 (2013).

[9] Shaklan, S. B. and Green, J. J., "Reflectivity and optical surface height requirements in a broadband coronagraph. 1.Contrast floor due to controllable spatial frequencies," Applied Optics 45, 5143–5153 (2006).

[10] Pueyo, L., Kay, J., Kasdin, N.~J., Groff T., McElwain, M., Give'on, A.,Belikov, R., "Optimal dark hole generation via two deformable mirrors with stroke minimization," Applied Optics, 48, 6296, (2009).

[11] Beaulieu, M., Abe, L., Martinez, P., Baudoz, P., Gouvret, C., Vakili, F., "High-contrast imaging at small separations: impact of the optical configuration of two deformable mirrors on dark holes," Monthly Notices of the Royal Astronomical Society, 469, 218 (2017).

[12] Baudoz, P., Mazoyer, J., Mas, M., Galicher, R., and Rousset, G., "Dark hole and planet detection: labora- tory results using the self-coherent camera," in [Ground-based and Airborne Instrumentation for Astronomy IV], Proc SPIE 8446, 84468C (2012).

[13] Zhou, P., Burge, J. H., "Analysis of wavefront propagation using the Talbot effect," Appl. Opt., 49, 5351 (2010).

[14] Baudoz, P., Galicher, R., Patru, F., Dupuis, O., Thijs, S., "Status and performance of the THD2 bench in multi-deformable mirror configuration", AO4ELT 2017 conference proceeding (2017).

[15] Rouan, D., Riaud, P., Boccaletti, A., Clénet, Y., and Labeyrie, A., "The four-quadrant phase-mask coron-agraph. i. principle," Publications of the Astronomical Society of the Pacific 112, 1479–1486 (2000).

[16] Singh, G., Martinache, F., Baudoz, P., Guyon, O., Matsuo, T., Jovanovic, N., and Clergeon, C., "Lyot- based Low Order Wavefront Sensor for Phase-mask Coronagraphs: Principle, Simulations and Laboratory Experiments," Publications of the Astronomical Society of the Pacific 126, 586 (2014).